© 2016. Published by The Company of Biologists Ltd | Development (2016) 143, 4665-4675 doi:10.1242/dev.144733

RESEARCH ARTICLE

Nodal and FGF coordinate ascidian neural tube morphogenesis

Ignacio A. Navarrete and Michael Levine*,‡

ABSTRACT

Formation of the vertebrate neural tube represents one of the premier examples of morphogenesis in animal development. Here, we investigate this process in the simple chordate *Ciona intestinalis*. Previous studies have implicated Nodal and FGF signals in the specification of lateral and ventral neural progenitors. We show that these signals also control the detailed cellular behaviors underlying morphogenesis of the neural tube. Live-imaging experiments show that FGF controls the intercalary movements of ventral neural progenitors, whereas Nodal is essential for the characteristic stacking behavior of lateral cells. Ectopic activation of FGF signaling is sufficient to induce intercalary behaviors in cells that have not received Nodal. In the absence of FGF and Nodal, neural progenitors exhibit a default behavior of sequential cell divisions, and fail to undergo the intercalary and stacking behaviors essential for normal morphogenesis. Thus, cell specification events occurring prior to completion of gastrulation coordinate the morphogenetic movements underlying the organization of the neural tube.

KEY WORDS: FGF, Nodal, Neurulation, Morphogenesis, Ascidian, Intercalation

INTRODUCTION

A central challenge of developmental biology is to understand how groups of cells self-organize into complex structures. It is generally assumed that cell specification events cause cells to express different sets of genes, which in turn determine their morphogenetic behaviors during development. Nevertheless, there are surprisingly few examples where cell specification has been directly linked to morphogenetic behaviors of individual cells (Ettensohn, 2013). Owing to its simplicity, the ascidian central nervous system (CNS) offers an outstanding opportunity to connect specification and morphogenesis in the context of chordate embryogenesis. Here, we investigate the role of fibroblast growth factor (FGF) and Nodal signaling in coordinating the early stages of neural tube morphogenesis in the ascidian *Ciona intestinalis*.

Molecular phylogenetic evidence suggests that tunicates such as *Ciona* are the closest living relatives of vertebrates (Delsuc et al., 2006). Indeed, the CNS of the ascidian tadpole has the same basic organization as that of vertebrates. It includes a sensory vesicle (simple brain) and nerve cord corresponding to the vertebrate spinal cord (Lemaire et al., 2002). Nevertheless, it is highly simplified, with just ∼330 cells comprising the CNS in mature larvae (Nicol and Meinertzhagen, 1991). In addition to its small cell number, *Ciona*'s fixed patterns of cleavage and invariant lineages (Conklin, 1905; Nishida, 1987) provide opportunities for understanding how individual cellular behaviors contribute to morphogenetic processes, such as formation of the neural tube.

Morphogenesis of the ascidian CNS follows a similar profile to that observed in vertebrate embryos (Nicol and Meinertzhagen, 1988a). During gastrulation, CNS progenitors come to occupy a flat neural plate on the dorsal side of the embryo. Neural tube formation (neurulation) begins immediately after the completion of gastrulation. Apical constriction causes bending of the neural plate, while a combination of oriented cell divisions and convergent extension movements results in a lengthening of the plate. Eventually, the lateral plate borders, aided by force from the surrounding epidermis (Ogura et al., 2011), meet at the dorsal midline together with the adjacent epidermis. Sequential contractions and rearrangements of neural-epidermal junctions cause a progressive posterior-to-anterior fusion of the epidermis overlying the neural tube following involution (Hashimoto et al., 2015).

Here, we investigate morphogenesis of the *Ciona* nerve cord. Considered in cross-section, it is composed of only four cells, including ventral and lateral ependymal cells that exhibit gene expression properties of the floor plate and lateral plate borders of the vertebrate neural tube, respectively (e.g. Corbo et al., 1997). These ventral and lateral cells are derived from the anterior vegetal (A-line) blastomeres (Fig. 1A). A-line cells contributing to the neural tube are segregated at the 44-cell stage when lateral A7.8 and medial A7.4 cells separate from their sisters, which form the primary notochord lineage (Nishida, 1987). Around this time A7.8 receives a Nodal signal from lateral b6.5 blastomeres, resulting in the induction of Snail and the repression of medial identity (Fig. 1B; Hudson and Yasuo, 2005; Hudson et al., 2007; Hudson et al., 2015; Imai et al., 2006). Disruption of this signal causes neural tube defects and misexpression of genes known to be involved in neural tube patterning and morphogenesis (Mita and Fujiwara, 2007; Mita et al., 2010).

Prior to gastrulation, both A7.8 and A7.4 undergo a mediolateral division to create the row of eight cells seen at the 110-cell stage (Fig. 1B). During gastrulation, these cells divide again, this time along the anterior-posterior axis, to create rows I and II of the neural plate at the mid-gastrula stage. Before this division, FGF induces subsequent activation of the mitogen-activated protein kinase (MAPK) signaling cascade in row I but not row II cells (Hudson et al., 2007). As a consequence of this differential MAPK activity, genes such as Mnx are activated only in row I, whereas others such as FoxB are restricted to row II (Hudson et al., 2007). Thus, at the mid-gastrula stage combinatorial FGF and Nodal signaling provides distinct identities to A-line cells comprising the presumptive neural tube (Fig. 1B).

We employed a combination of time-lapse live imaging and lineage-specific genetic perturbations to investigate how Nodal and FGF signals coordinate movements of lateral and ventral neural progenitor cells during neurulation. We find that FGF signaling is

Department of Molecular and Cell Biology, Division of Genetics, Genomics and Development, University of California, Berkeley, CA 94720, USA.
*Present Address: Lewis-Sigler Institute, Department of Molecular Biology, Princeton University, Princeton, NJ 08544, USA.

‡Author for correspondence (msl2@princeton.edu)

M.L., 0000-0001-7519-0396

Received 13 September 2016; Accepted 21 October 2016

Development (2016) 143, 4665-4675 doi:10.1242/dev.144733

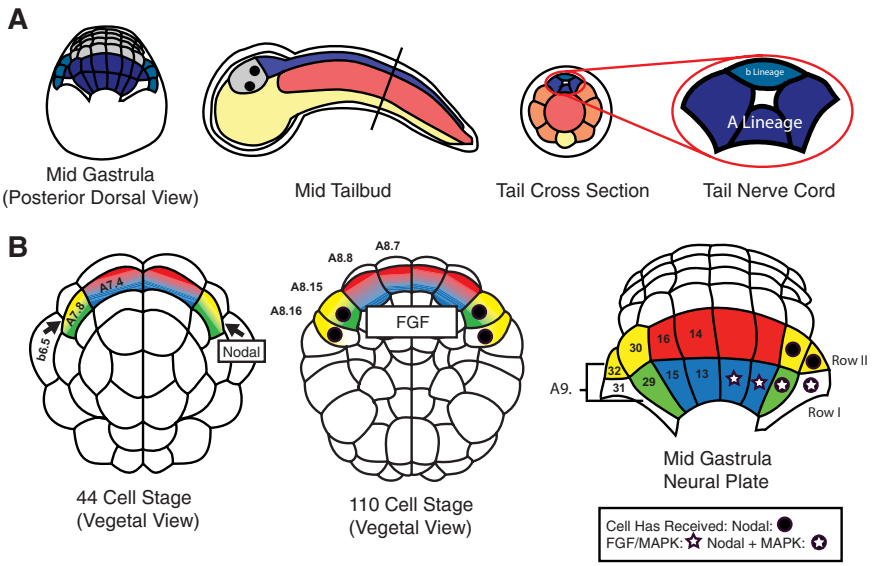

Fig. 1. *Ciona* A-line neural development. (A) Tail nerve cord lineages at mid-gastrula and mid-tailbud stages. Dark blue cells represent the A-lineage, which contributes to the ventral and lateral nerve cord; light blue represents b-line cells contributing to the dorsal nerve cord. Gray represents a-line neural cells at the mid-gastrula stage and the a-line-derived anterior sensory vesicle in tailbud embryo. Other tissues in the tailbud diagram are notochord (red), muscle (orange), endoderm (yellow) and epidermis (white). Lateral view of tailbud is a mid-sagittal section. Black bar shows location of tail cross-section. (B) Specification of A-line neural cells by Nodal and FGF signals. On the left side, blastomeres are labeled according to ascidian nomenclature. Colors represent A-line neural cell lineages (red, medial row II; yellow, lateral row II; blue, medial row I; green, lateral row I) and symbols represent signaling as shown in the key. A9.31 contributes to the tail muscles and is therefore uncolored. At the 44-cell stage, Nodal originating from the b6.5 blastomere signals to A7.8 but not A7.4. At the 110-cell stage an FGF signal of unknown origin is transduced, ultimately leading to MAPK activation in row I but not row II at the mid-gastrula stage.

essential for intercalary movements leading to midline convergence of ventral 'floor plate' cells. We also present evidence that Nodal signaling is required for proper stacking of lateral cells. In the absence of both FGF and Nodal signaling, neural progenitors exhibit a default behavior of sequential anterior-posterior oriented divisions. These results suggest a direct impact of FGF and Nodal on the cellular behaviors underlying neurulation.

RESULTS

Live imaging of neurulation

To explore how cells of the posterior CNS move and divide during neurulation, we used time-lapse confocal microscopy to visualize the nuclei of these cells starting at the mid-gastrula stage. Nuclei were labeled by electroporation of a FoxB>H2B:YFP reporter gene (Imai et al., 2009), which recapitulates endogenous FoxB expression in A7.4, A7.6 and A7.8, and later in the lateral epidermis during neurulation (Imai et al., 2004; Fig. S1). In a control embryo co-electroporated with FoxB>H2B:YFP and FoxB>*lacZ* we traced cells until the mid-tailbud stage (Fig. 2A-D,I; Fig. 3; Movie 1; Fig. S2). The results obtained were consistent with those from other time-lapse experiments (Table S1).

A-line neural cells exhibit asynchronous cycles of division that can be assigned to different groups based on timing (Nicol and Meinertzhagen, 1988b). Cells within a group enter and exit mitosis within a ~15 min time window that is distinct from cells in earlier or later dividing groups. The first group of cells to divide is A9.16 and A9.14 belonging to medial row II. This is followed by medial row I cells (A9.15 and A9.13) and the lateral cells A9.29 and A9.32; A9.30 is the last to divide (Fig. 3).

Starting at the mid-gastrula stage neural progenitors begin to organize into lateral and ventral regions of the future neural tube (Fig. 2, see also Fig. 9E). The lateral walls of the tube are initially formed by the posterior movements of A9.30, A9.29, and A9.32 derivatives relative to A9.16 derived cells; we will refer to this collective set of movements as 'lateral stacking'. During the transition from mid to late gastrula, A9.29 moves posterior to A9.30 and underneath A9.32, separating these cells. Simultaneously, A9.30 begins to slide behind A9.16, a movement that is not completed until both cells have divided. Finally, derivatives of A9.32 eventually move posterior to A9.29 progeny. Each tenth generation lateral cell remains in contact with its sister cell, resulting in a pair of lateral stacks that extend from anterior to posterior regions of the neural plate at the early neurula stage (Fig. 2B,F). To form the ventral 'floor plate' A9.13 and A9.15 derivatives converge at the midline, intercalate and separate from their sisters (Fig. 2B,C; Fig. S2A). The anterior-most floor plate cell arises from the left A10.26 blastomere in some embryos, and the right A10.26 cell in others (Table S1). These movements are consistent with those described by Nicol and Meinertzhagen (1988a).

Time-lapse imaging reveals that the ventral floor plate is formed entirely from derivatives of A9.13 and A9.15, and, consequently, the progenitors of this structure are already segregated at the mid-gastrula stage (Fig. 2). Previous studies suggested that A9.14 derivatives also contribute to the floor plate (Cole and Meinertzhagen, 2004; Nicol and Meinertzhagen, 1988a). Instead, we find that they contribute exclusively to the lateral regions of the posterior sensory vesicle at the mid-tailbud stage. A9.14 derivatives are among the first A-line neural cells to enter the 11th generation (Fig. 2C,G; Fig. S5A,B), and by the late neurula stage they have moved in front of A9.16 derivatives to form the anterior-most portion of the A-line-derived lateral neural tube (Fig. 2D,H). At the initial tailbud stage, these cells divide in a dorsal-ventral orientation to enter the 12th generation. We observe two additional deviations from the published fate maps. First, A9.29 derivatives form most of the cells comprising the lateral neural tube posterior to the visceral ganglion, providing eight cells on each side at the mid-tailbud stage. Second, the anterior daughter of A9.32 (A10.64) eventually leaves the neural tube and migrates towards the trunk (Fig. 2J).

FGF is essential for midline convergence of A9.13 and A9.15 derivatives

FGF signaling distinguishes the identities of progenitor cells located in rows I and II of the neural plate (Hudson et al., 2007). Inhibition of FGF at the 110-cell stage causes row I cells to lose expression of row I markers and ectopically express genes normally restricted to row II. Given that ventral cells arise from row I, we sought to determine whether FGF is also required for the intercalary behavior of these cells. Towards this goal, we selectively expressed a dominant-negative form of the FGF receptor (dnFGFR) in the A-line neural plate using the FoxB enhancer. The consequences were examined in living embryos using time-lapse confocal microscopy (Fig. 4A-C; Movie 2). We observed a number of

Development (2016) 143, 4665-4675 doi:10.1242/dev.144733

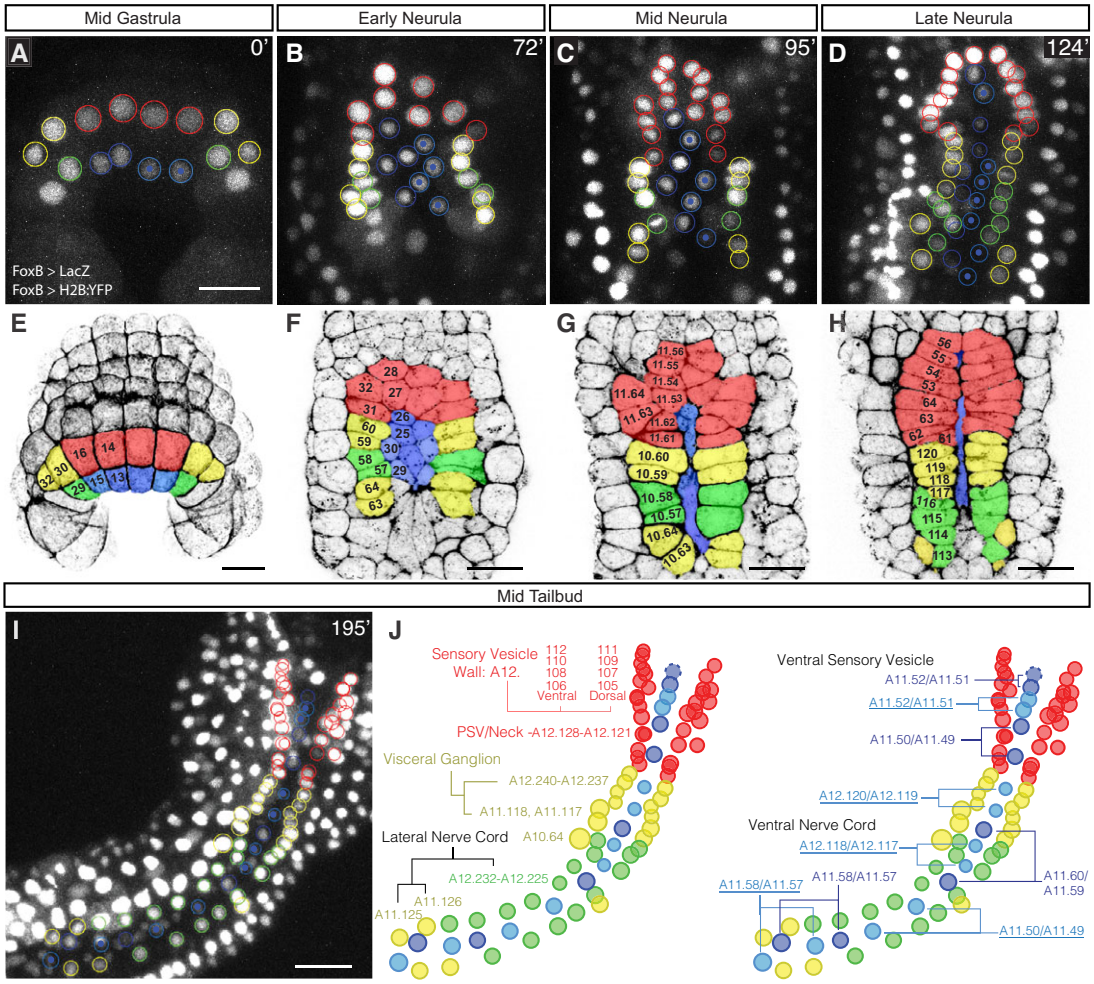

Fig. 2. Revised A-line neural lineage. (A-D,I) Time-lapse images of an embryo electroporated with FoxB>H2B:YFP and FoxB>*lacZ* from mid-gastrula stage to mid-tailbud stage. Circled cells belong to the A-line neural lineage. Cells were manually traced and labeled with Fiji trackmate plugin. Where cells from the left and right sides of the embryo mix, right-side cells are indicated by a dot within the nucleus. (E-H) False-colored images of phalloidin-stained embryos labeled with cell identities corresponding to the cells tracked in A-D. Embryos were electroporated with FoxB>H2B:Cherry to aid in cell identification and *lacZ* as a control for later experiments. (E) Three-dimensional projection of a mid-gastrula-stage embryo. Labeled cells are A-line of the ninth generation. (F-H) Single confocal slices from embryos at the indicated stages. (F) Labeled cells are of the tenth generation. (G) Labeled cells are of the tenth or 11th generation, as indicated. (H) Labeled cells are of the 11th generation. (J) Identities of A-line neural cells tracked to the mid-tailbud stage. Dashed circle represents the presumed location of A11.52, which moves beyond stack depth at 182 min. The following deviations from the published fate map were observed in this and other time-lapse experiments: A9.14 contributes to lateral walls (7/7), sixteen A9.29 derivatives at late neurula stage (6/6), anterior migration of A10.64 (3/3, unable to continuously trace in other experiments). Underlined labels indicate cells derived from right-side blastomeres. Colors reflect the lineage of each cell as in Fig. 1B. PSV, posterior sensory vesicle. Scale bars: 25 µm.

changes relative to control embryos. First, all medial cells (A9.14, 16, 13 and 15) divide within the same 15-min time window (Fig. 4B; compare with Fig. 3) and enter the 11th generation before lateral cells. Second, derivatives of A9.13 and A9.15 fail to converge at the midline, and retain contacts with their sister cells (Fig. 4C; Fig. S5C,D). Phalloidin staining of mutant embryos confirmed that A9.13 and A9.15 derivatives fail to intercalate, and instead line up on either side of the midline, mimicking the normal behavior of A9.14 derivatives (Fig. 4D-F). At the mid-neurula stage, at least one daughter of A9.13 reached the 11th generation in 87% of all embryos examined, compared with just 3% in control embryos (Fig. 5H).

To test whether floor plate convergence requires FGF signaling beyond the initial specification of row I fates, we inhibited signaling at the mid-gastrula stage. We began by using the MEK inhibitor UO126 to block MAPK signaling. As expected, treatment at the 110-cell stage caused intercalation defects consistent with the adoption of medial row II behaviors by A9.13 and A9.15 derivatives (Fig. 4F). This treatment also seemed to cause a slight delay in overall development, which probably accounts for the reduction of precocious divisions observed relative to electroporation of FoxB>dnFGFR. By contrast, UO126 treatment at the mid-gastrula stage resulted in only occasional defects in the convergence of A9.13 and A9.15 derivatives, suggesting that the requirement for MAPK signaling is confined to specification at the 110-cell stage. To test for MAPK-independent FGF signaling, we expressed the dominant-negative receptor using an Mnx enhancer active in A9.13 and A9.15 derivatives starting at the mid-gastrula stage (Fig. S3A). This caused convergence defects in more than 50% of embryos examined, suggesting that MAPK-independent FGF signaling may play a continuing role in floor plate intercalation (Fig. 4F).

We next sought to determine whether FGF signaling is sufficient to induce intercalary behaviors in medial row II cells, which normally form lateral regions of the sensory vesicle. To do so, we expressed a

Development (2016) 143, 4665-4675 doi:10.1242/dev.144733

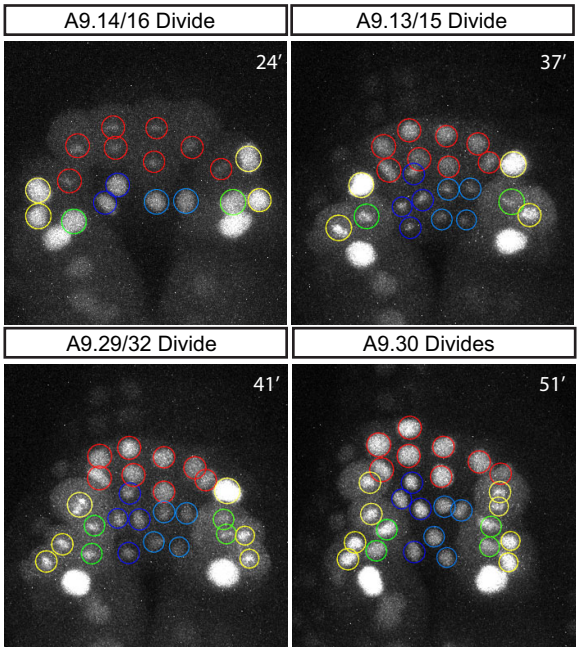

Fig. 3. Timing of entry into the tenth generation. Stills from time-lapse imaging of a FoxB>H2B:YFP- and FoxB>*lacZ*-electroporated embryo (Movie 1) showing A-line cells entering the tenth generation at the indicated time points. In control embryos, medial row II cells always divide first (n=7/7) and A9.30 is always last (n=7/7). Colors reflect the lineage of each cell as in Fig. 1B.

constitutively active form of the *Ciona* MEK kinase (Mansour et al., 1994) using the FoxB enhancer (Fig. S3B). Cell identities were monitored using the Mnx enhancer attached to a H2B:Cherry reporter. Misexpression of activated MEK caused ectopic activation of the Mnx reporter, consistent with a transformation of row II cells to row I identity (Fig. 5E,F). Time-lapse imaging of mutant embryos revealed multiple changes in cell behavior (Fig. 5A-C; Movie 3). In contrast to control embryos (Fig. 3), divisions of medial row II cells (A9.14/A9.16) occurred within the same 15-min period as divisions of medial row I (A9.13/A9.15) (Fig. 5B). Furthermore, derivatives of A9.14/A9.16 did not enter the 11th generation prior to the mid-neurula stage (Fig. 5C,H). Importantly, we also observed midline convergence of A9.14 derivatives, whereby sister cells lose their contacts during rearrangement (Fig. 5C; Fig. S5E,F). This behavior is in stark contrast to control embryos, in which A9.14 derivatives remain confined to either side of the midline (e.g. Fig. 2C,G; Fig. 5E). Midline convergence of A9.14 derivatives is clearly visualized in fixed embryos stained with phalloidin (Fig. 5D,F).

We next investigated whether FGF signaling induces ventral cell behaviors by transcriptionally regulating specific target genes. To do so, we overexpressed a constitutively active form of the FGF/MAPK transcriptional effector Elk:VP64, which is a member of Ets family of transcription factors (Gainous et al., 2015). Co-electroporation of embryos with a FoxB>Elk:VP64 transgene and Mnx>H2B:Cherry reporter resulted in ectopic expression of the Mnx reporter in A9.14 and A9.16 derivatives (Fig. 5G), as seen with constitutive FGF signaling (Fig. 5F). Ectopic expression was also observed at a lower frequency in other A-line neural cells. Changes in cell behaviors were also detected, including delays in division and midline convergence of A9.14 derivatives (Fig. 5G,H), consistent with FGF mediating midline convergence via transcriptional targets.

It is possible that induction of midline convergence of row II cells is a passive response caused by the delay of cell division and surrounding forces in the embryo. To explore this possibility, we used the DNA polymerase inhibitor aphidicolin to prevent row II cells from entering the 11th generation, mimicking the delay in division caused by MAPK activation (Fig. 6A). We then measured the length of membrane spanning the midline across row II derivatives, reasoning that a lengthening of this span will necessarily accompany convergence of cells across the midline (Fig. 6C,D). Comparing aphidicolin-treated embryos with and without MAPK activation, we found that MAPK activation induces midline convergence beyond any possible effects of delaying cell division alone (Fig. 6B).

To better visualize midline convergence we used the FoxB enhancer to drive a membrane-targeted YFP reporter gene (YFP-CAAX) (Fig. 7A,B; Movies 4 and 5). We found that in both normal ventral cells (row I) and 'activated' row II cells, midline rearrangements occur by contraction of localized junctions resulting in the separation of sister cells through neighbor exchange (also known as a T1 transition). Intercalation begins when mediolateral junctions spanning sister cells contract causing cells to the left and right sides to come into contact. The process is completed when an anterior-posterior oriented junction is established between these cells. Two additional points are worth noting. First, tenth generation A9.14/16-derived cells transformed to a medial row I identity by MAPK activation are larger than row I cells, as is the case in unperturbed embryos (Nicol and Meinertzhagen, 1988a), suggesting a source of asymmetry not determined by MAPK signaling alone. Second, rearrangement of the converted cells takes longer than that of normal row I cells.

Nodal is required for lateral stacking

Perturbation of FGF signaling had no apparent impact on the stacking of lateral cells (compare Fig. 2C,G with Fig. 4C,E and Fig. 5C,D). We suspected that the behavior of these cells might be controlled by the lateral Nodal signal that distinguishes them from their medial counterparts before the 64-cell stage (Hudson et al., 2007). To test this idea, we performed time-lapse imaging on embryos electroporated with FoxD>Lefty, which inhibits Nodal signaling and causes lateral cells to express medial marker genes (Mita and Fujiwara, 2007).

Inhibition of Nodal signaling caused changes in both the timing of division and cell organization (Fig. 8A-D; Movie 6). In contrast to control embryos (Fig. 3), all row II cells entered the tenth generation within the same 15-min window (Fig. 8B,C) and entered the 11th generation prior to the mid-neurula stage. Lateral stacking was defective (Fig. 8D; Fig. S5G,H) with A9.30, A9.29 and A9.32 derivatives failing to arrange themselves posterior to A9.16 on either side of the embryo. A9.14 and A9.16 derivatives made their usual oriented divisions, whereas A9.29-derived cells seemed to join the intercalary behavior of A9.15 and A9.13 derivatives, causing these movements to be disorganized.

The outcome of these altered behaviors is easily observed with phalloidin staining, which allowed us to quantify the phenotype using two diagnostic features: the presence of six columns of A-line-derived cells at the mid-neurula stage and the addition of A9.29 derivatives to the floor plate, causing it to have twelve rather than eight cells (Fig. 9A-D). The FoxD enhancer drives expression in A5.1, A5.2, and B5.1 blastomeres starting at the 16-cell stage (Mita and Fujiwara, 2007). To determine whether Nodal signaling is required beyond the early gastrula stage, we expressed Lefty using the later-acting Etr enhancer. This had no effect on stacking, suggesting that Nodal is not required during these movements (Fig. S4A-D).

Development (2016) 143, 4665-4675 doi:10.1242/dev.144733

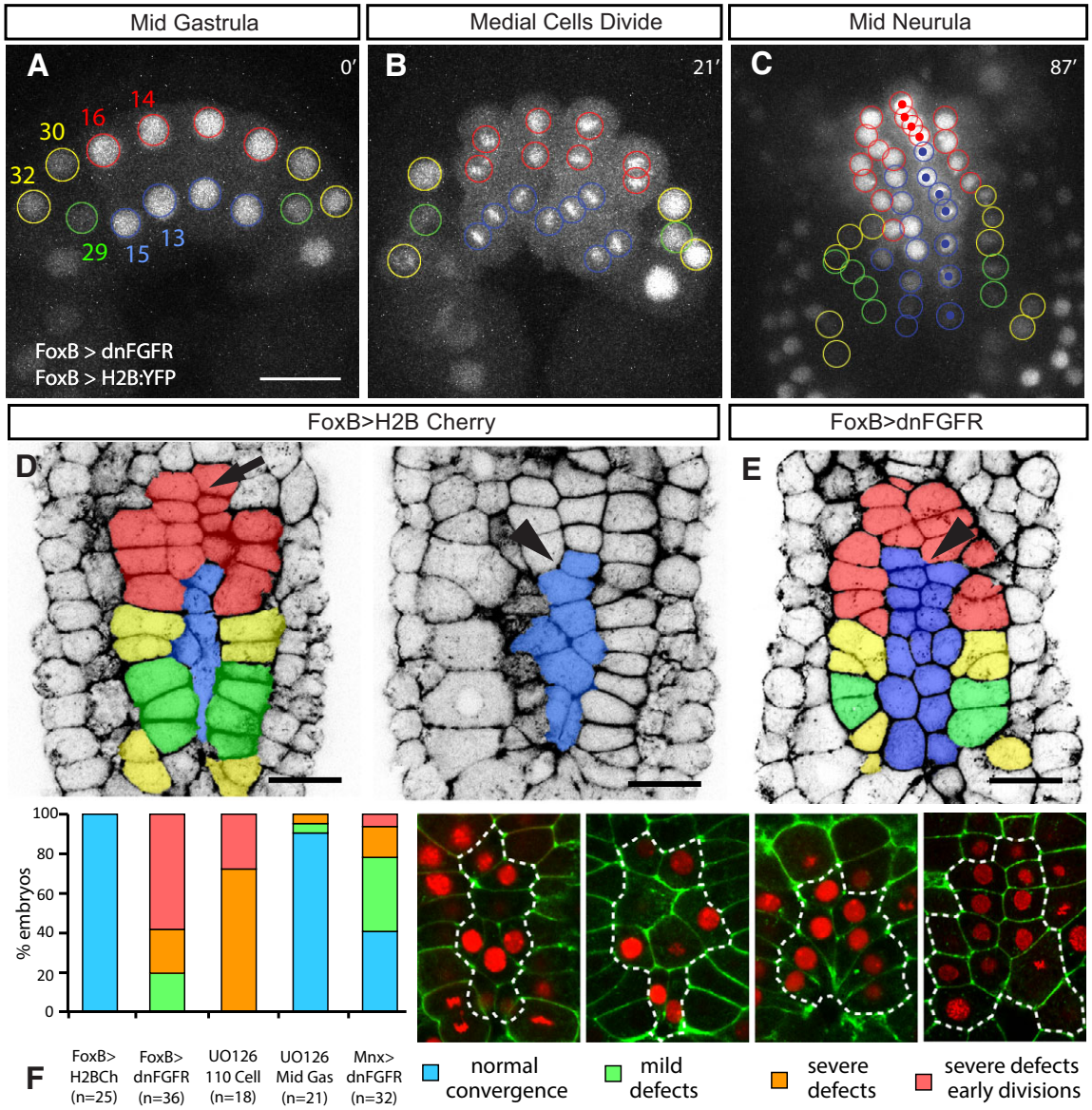

Fig. 4. FGF/MAPK is required for midline convergence of floor plate cells. (A-C) Time-lapse confocal microscopy of an embryo co-electroporated with FoxB>dnFGFR and FoxB>H2B:YFP. Cell lineages are color coded as in Fig. 1 and right-side nuclei at the midline are indicated with a spot. (B) Derivatives of A9.14, 16, 13 and 15 divide simultaneously (*n*=3/3). (C) At mid-neurula stage, most A9.13- and A9.15-derived cells have divided twice and failed to cross the midline (*n*=3/3). (D,E) False-colored phalloidin-stained mid-neurula embryos electroporated with FoxB>H2B:Cherry alone (D) or FoxB>dnFGFR together with FoxB>H2B:Cherry (E). In control embryos, A9.14 derivatives are confined to either side of the midline (arrow) whereas A9.13 and A9.15 derivatives converge, interrupting the membrane spanning the midline (arrowhead). In embryos electroporated with FoxB>dnFGFR, this midline span continues between left and right A9.13- and A9.15-derived cells (arrowhead). (F) Quantification of phenotypes for the indicated treatment. When convergence is normal, multiple floor plate cells are in contact with lateral cells from the left and right sides. Mild defects are defined by some rearrangement of floor plate cells with one or fewer cells spanning left and right lateral cells. Severe defects occur when floor plate cells are entirely confined to the side of the embryo where they originated; early divisions occur when one or more of these cells has entered the 11th generation by the mid-neurula stage. FoxB>H2B:Cherry total consists of 12 embryos co-electroporated with FoxB>*lacZ* and 13 embryos treated with DMSO at the 110-cell stage. Totals are from two independent experiments. Dashed line outlines A9.13 and A9.15 derivatives in the images in F. Scale bars: 25 µm.

To better understand the cellular behaviors underlying lateral stacking, we used the membrane-targeted reporter YFP-CAAX to visualize the consequences of FoxD>Lefty electroporation in live embryos (Fig. 9E; Movie 8). In contrast to control embryos, A9.29 failed to insert between A9.30 and A9.32. Furthermore, A9.30 remains adjacent to and divides simultaneously with A9.16, such that daughters of both cells end up side by side rather than aligned along the anterior-posterior axis. Together, these changes are sufficient to explain the defects in lateral stacking already apparent at the early neurula stage (Fig. 9E, 45′).

To test whether Nodal signaling was sufficient to induce stacking behavior, we ectopically expressed Nodal in vegetal regions using a FoxD>Nodal fusion gene (see Mita and Fujiwara, 2007). Nuclei were visualized with a Snail>H2B:YFP reporter gene (Fig. 8E,F; Movie 7; Fig. S5I,J). Nodal signaling induces Snail expression, and ectopic expression of Nodal results in ectopic activation of Snail in medial cells. Live imaging revealed that the timing of entry into the tenth generation was uncoordinated and overall development was delayed. Nevertheless, stacking of lateral cells appeared mostly normal. Furthermore, medial row I cells failed to

Development (2016) 143, 4665-4675 doi:10.1242/dev.144733

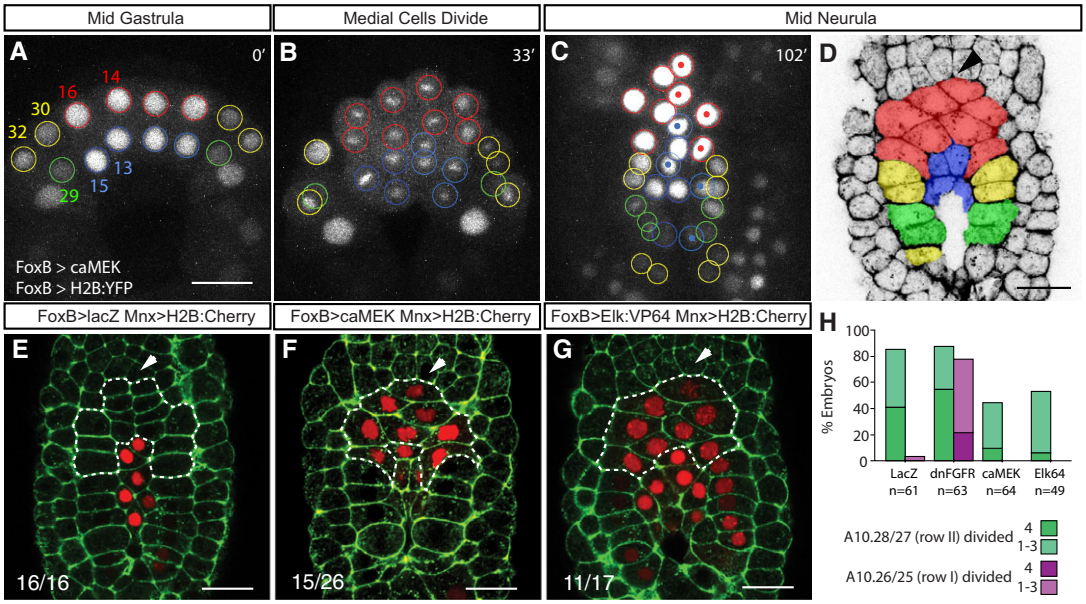

Fig. 5. FGF/MAPK acting through Ets/Elk family transcription factors delays cell division and promotes midline convergence of medial cells. (A-C) Time-lapse confocal microscopy of an embryo co-electroporated with FoxB>caMEK and FoxB>H2B:YFP. (B) Derivatives of A9.14, 16, 13 and 15 divide simultaneously (*n*=6/7). (C) At mid-neurula stage, A9.14 and A9.16 derivatives (red) have failed to enter the 11th generation and have converged towards the midline (*n*=5/7). (D) False-colored phalloidin-stained mid-neurula embryo electroporated with FoxB>caMEK and FoxB>H2B:Cherry. Arrowhead indicates where midline membrane is interrupted by A9.14 derivative. (E-G) Mid-neurula-stage embryos electroporated with the indicated transgenes and stained with phalloidin. Dashed line outlines A9.14/A9.16 derivatives. (E) Mnx reporter is limited to A9.13- and A9.15-derived floorplate cells. (F,G) Ectopic Mnx expression is seen in A9.14 and A9.16 derivatives. In both cases, these cells also interrupt the midline membrane (arrowheads). Floorplate cells are deeper within embryo. Number of embryos that exhibit ectopic Mnx reporter expression in combination with delayed division and midline convergence of A9.14/A9.16 derivatives is shown. Totals are from two independent experiments. (H) Quantification of A9.14 and A9.13 derivatives that have entered the 11th generation by the mid-neurula stage. Embryos were electroporated with FoxB driving the indicated gene and FoxB>H2B:Cherry to aid quantification. Totals are from two independent experiments. Scale bars: 25 µm.

properly intercalate and medial row II cells failed to enter the 11th generation by the mid-neurula stage.

The results described above suggest that FGF controls intercalation of medial cells, whereas Nodal controls stacking of lateral cells. As a further test of this possibility we performed time-lapse imaging of embryos that lack both signals in the neural plate (i.e. co-expression of FoxD>Lefty and FoxB>dnFGFR) (Fig. 10A-C; Movie 9). In this experiment, all cells of the A-line neural plate entered the tenth generation within the same 15-min window and entered the 11th generation by the mid-neurula stage. All cell divisions are oriented along the anterior-posterior axis, and there is an absence of the cellular rearrangements required for the formation of lateral stacks and midline intercalation (Fig. 10C; Fig. S5K,L).

We next investigated whether all A-line neural cells would participate in midline convergence if MAPK were activated in the absence of Nodal. To test this, we performed live imaging on embryos lacking Nodal but misexpressing a constitutively activated form of MEK (co-expression of FoxD>Lefty and FoxB>caMEK transgenes) (Fig. 10D-F; Movie 10). Under these conditions, Mnx is expressed in all A-line neural cells suggesting a complete transformation to medial row I identity (Fig. S4E). As expected for medial row I derivatives, all cells entered the tenth generation within the same 15 min window, and did not enter the 11th generation by the mid-neurula stage. There is a dramatic midline convergence of both row I and row II derivatives, including separation of lateral sister cells that normally undergo stacking (Fig. 10F; Fig. S5M,N). These results are consistent with the idea that FGF and Nodal independently specify intercalary and stacking behaviors of neural plate progenitor cells (see Discussion).

DISCUSSION

We have presented evidence that Nodal and FGF signals deployed before completion of gastrulation coordinate the morphogenetic behaviors of A-line neural progenitor cells during neurulation (Fig. 10G). FGF signaling is required for midline convergence of floor plate cells and is sufficient to induce intercalary behaviors in A-line cells not exposed to Nodal. Nodal signaling is required for proper stacking of lateral cells and inhibition of this signal causes these cells to adopt the behavior of their medial counterparts. In the absence of both FGF and Nodal signals, neural tube progenitors adopt default behaviors that are typical of those seen for the progenitors of the sensory vesicle.

Revised lineage of A-line neural cells

Time-lapse live imaging revealed that the organization of A-line cells during neurulation is simpler than previously thought. Especially striking is the observation that the floor plate is derived entirely from A9.13 and A9.15, whereas A9.14 contributes only to the sensory vesicle. It seems probable that A9.14 gives rise to the lateral portions of the ‘middle sensory vesicle’ identified by Nakamura et al. (2012), which is consistent with studies suggesting that the photoreceptors of the ocellus are derived from the medial A-lineage (Gainous et al., 2015; Taniguchi and Nishida, 2004). It therefore appears that the basic subdivision of the posterior CNS into middle sensory vesicle, posterior sensory vesicle, visceral ganglion, lateral nerve cord and floor plate is already established at the mid-gastrula stage, similar to the time when CNS patterning becomes evident in vertebrates (Lumsden and Krumlauf, 1996).

Our live-imaging studies suggest that the precise order of medial convergence in the floor plate might not be fixed, but is somewhat

Development (2016) 143, 4665-4675 doi:10.1242/dev.144733

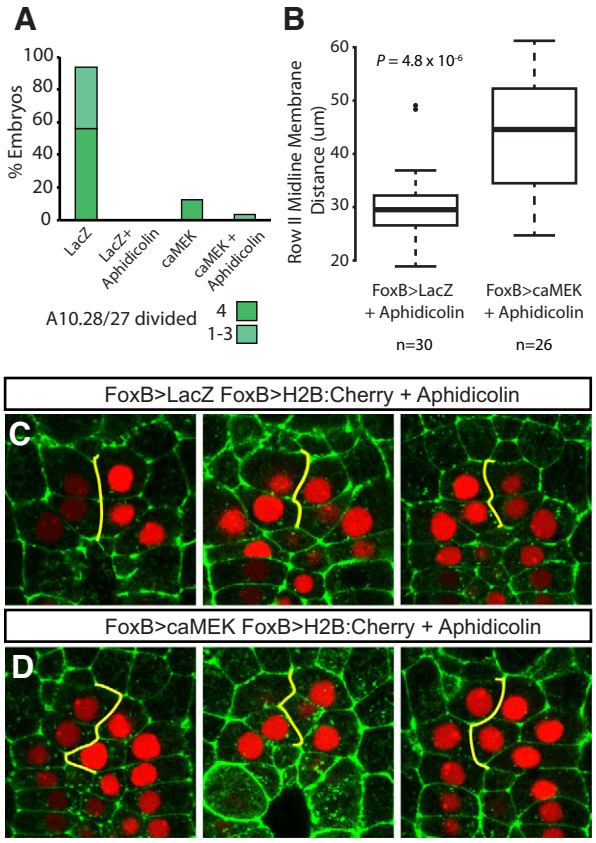

Fig. 6. Cell cycle delay is not sufficient for full midline convergence. (A) Quantification of A9.14 derivatives that have entered the 11th generation by the mid-neurula stage. Embryos were electroporated with FoxB driving the indicated gene and FoxB>H2B:Cherry to aid quantification. Aphidicolin treatment was carried out at the late gastrula stage. Total number of embryos counted from four independent experiments: *lacZ*: 16, *lacZ*+aphidicolin: 30, caMEK: 16, caMEK+aphidicolin: 28. (B) Box plot summary of midline membrane span length between A9.14 derivatives at mid-neurula stage. Measurements were performed manually with ImageJ software. Statistical significance calculated with Wilcoxon two-sample test. (C,D) Examples of membrane span traces (yellow lines) used to create the data shown in B. Embryos were electroporated with the indicated transgenes and treated with aphidicolin.

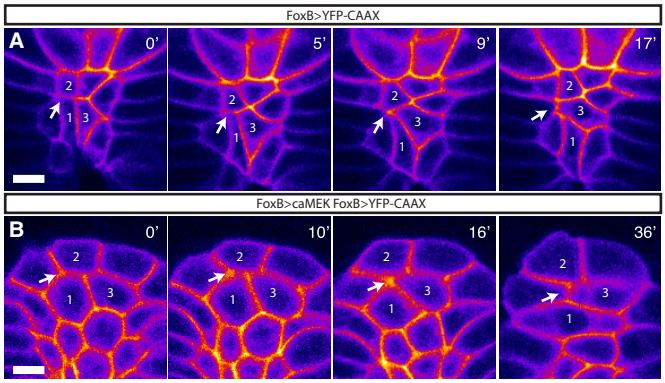

Fig. 7. Junction rearrangement during midline convergence. Stills from time-lapse live imaging of embryos electroporated with the indicated transgenes. Numbers mark the same cell from one frame to the next with cell 3 inserting between cells 1 and 2 in both cases. Arrow indicates rearrangement of junction configuration between cells 1 and 2. Pseudo-color look-up table was chosen to increase membrane visibility. (A) Intercalation of medial row I cells. 1: A10.25 (left), 2: A10.26 (left), 3: A10.25 (right). (B) Intercalation of medial row II cells. 1: A10.27 (left), 2: A10.28 (left), 3: A10.27 (right). Scale bars: 10 µm.

variable among different embryos. Similar variability is observed for the intercalation of the notochord during the convergence of left and right progenitors across the midline (Miyamoto and Crowther, 1985; Nishida, 1987). We are also curious about the final fate of A10.64 derivatives, which migrate anteriorly along the neural tube as the tail extends. It is conceivable that these cells respond to the same migratory cues as the BTN cells, which possess some of the properties of neural crest derivatives (Stolfi et al., 2015). It is also possible that A10.64 cells correspond to Islet-positive neurons of the visceral ganglion (Stolfi and Levine, 2011) rather than A10.57.

FGF/MAPK signaling and cellular morphogenesis

FGF signaling is crucial for early vertebrate development and neural patterning (Böttcher and Niehrs, 2005) and is involved in numerous cell specification events during ascidian embryogenesis (e.g. Bertrand et al., 2003; Davidson et al., 2006; Wagner and Levine, 2012). Our study demonstrates that FGF signaling also controls the timing of cell divisions and midline convergence of medial row I cells. Activation of canonical FGF/MAPK signaling or the downstream ETS-containing Elk transcriptional effector is sufficient to delay cell division and induce midline convergence, whereas inhibition of MAPK signaling after specification of medial row I fates does not alter the behavior of these cells. Together, these results suggest that FGF/MAPK signaling during gastrulation is sufficient to simultaneously induce a floor plate identity and intercalary behaviors. Nevertheless, normal intercalation does seem to rely on non-canonical FGF signaling after specification is complete. This situation is reminiscent of notochord morphogenesis, whereby canonical FGF/MAPK signaling at the 44-cell stage specifies notochord identity (Kim and Nishida, 2001; Nakatani and Nishida, 1997) but subsequent non-canonical FGF signaling is required for convergent extension (Shi et al., 2009). Future studies will hopefully identify the target genes responsible for the detailed cell behaviors underlying intercalation of the floorplate, including detachment of sister cell contacts. It will also be important to determine how this particular response to FGF signaling is achieved in contrast to the many other instances of MAPK-mediated FGF signaling during *Ciona* embryogenesis. FoxB is known to prevent notochord induction in response to FGF in the A-line neural lineage (Hashimoto et al., 2011), but it remains to be seen whether FoxB is sufficient to promote the development of floor plate cells in response to FGF.

Active junction contraction

There is evidence that diverse instances of convergent extension employ similar mechanisms of junction contraction (Shindo and Wallingford, 2014). We have provided evidence that such contraction might also underlie intercalation of the *Ciona* floor plate. However, there are also differences. For example, *Flamingo* (*Celsr*) and *Prickle* regulate intercalary behavior through the planar cell polarity pathway (Nishimura et al., 2012; Takeuchi et al., 2003), but are absent in the floor plate. Curiously, these genes are expressed in the lateral neural plate, which undergoes stacking rather than convergence (Mita et al., 2010; Noda and Satoh, 2008).

We have also presented evidence that floor plate midline convergence is an active process, and not merely a passive consequence of delayed cell divisions. Nonetheless, a delay in division might contribute to the robustness of intercalation. Evidence that floor plate convergence is an active process agrees

Development (2016) 143, 4665-4675 doi:10.1242/dev.144733

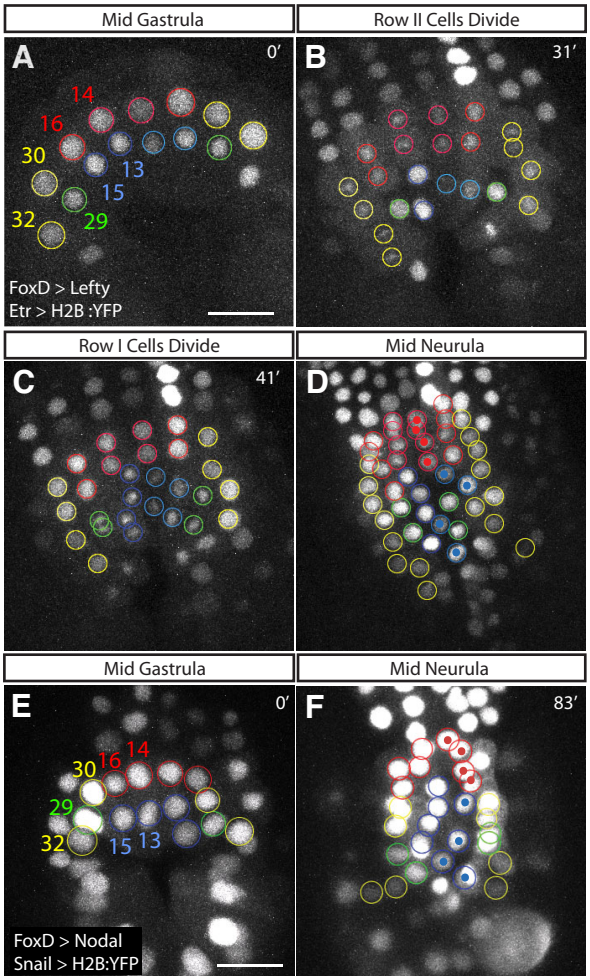

Fig. 8. Nodal influences timing of division and is required for proper lateral stacking during neurulation. Stills from time-lapse imaging visualizing H2B:YFP. Cell lineages are color coded as in Fig. 1 and right-side nuclei at the midline are indicated with a spot. (A-D) Embryo electroporated with FoxD>Lefty and Etr> H2B:YFP. (B,C) All cells belonging to row II divide simultaneously followed by all cells in row I (n=5/5). (D) Lateral stacking of A9.32, 30, 29 and 16 is disrupted and lateral row II cells have prematurely reached the 11th generation (n=6/6). (E,F) Embryo electroporated with FoxD>Nodal and Snail>H2B:YFP. (F) A9.14/16 cells (red) have failed to enter 11th generation by mid-neurula stage and lateral stacking of A9.32, 30, 29 and 16 is normal (n=3/3). Scale bars: 25 µm.

with previous work showing that the tail nerve chord undergoes extension even in the absence of notochord differentiation and extension (Di Gregorio et al., 2002).

Self-organization of the neural tube

Morphogenesis of the *Ciona* neural tube provides a simple and attractive model for understanding how complex structures arise from an initially undifferentiated group of cells. Indeed, we have shown that in the absence of FGF and Nodal signals all neural tube progenitors undergo the same program of oriented cell divisions as typically seen for the sensory vesicle. It is only through the influence of external signals that cells within this group adopt the unique behaviors necessary for proper neural tube morphogenesis. These signaling events are also used for cell specification, suggesting that transient cell states influence morphogenetic behaviors of cells en route to their ultimate identities. Intriguingly, we find that the signals establishing these states are deployed prior to the completion of gastrulation, but the behaviors they confer are not fully realized until the onset of neurulation. Understanding how these states arise and in turn influence cellular morphogenesis promises to be a continuing challenge in the quest to discover how anatomy is encoded in the genome.

MATERIALS AND METHODS

Molecular cloning

FoxB, Snail, and ETR regulatory sequences have been reported previously (Corbo et al., 1997; Imai et al., 2009; Veeman et al., 2010). The Mnx −5 kb regulatory sequence was amplified from genomic DNA using the primers F-TATGGCGCGCCTCCTGATGTGACGGATTTATGACTG, R-TATGCGGCCGCTAGCATCATTTTAAATCTTAAATATCAAAGGTTC and cloned into a H2B:Cherry-containing expression vector using *Not*I and *Asc*I restriction sites. dnFGFR and Elk:VP64 were digested from Dmrt4>dnFGFR (Wagner and Levine, 2012) and Zicl>ElkLVP64 (Gainous et al., 2015) using *Not*I and *Blp*I and cloned downstream of the FoxB and Mnx enhancers. A clone of the *Ciona* MEK1/2 gene (citb42j03) was modified to produce the amino acid changes S116D and S220E using the primers TATGATCTTGTCCCTACAAACTCGTTGGCCATATCGTCGATCAGTTGCCCGCTCAC and GTGAGCGGGCAACTGATCGACGATATGGCCAACGAGTTTGTAGGGACAAGATCATA and the Stratagene quick-change site-directed mutagenesis procedure. The modified coding sequence was then amplified using the primers F-TATGCGGCCGCGATGCCTCCTAAACGTAAGTTAAACC, R-TATGAATTCTTAATCAGGTACAGTGTCTGGACT and cloned into a vector containing the FoxB enhancer using *Not*I and *Eco*RI restriction sites. FoxD>Lefty and FoxD>Nodal (Mita and Fujiwara, 2007) were generously obtained from Shigeki Fujiwara. To construct Etr>Lefty, the Lefty coding sequence was amplified with F-TATGCGGCCGCGATGGCCCGGGCGAA and R-GGATTTCCTTACGCGAAATACG, digested with *Not*I/*Eco*RI and cloned into a vector containing the Etr enhancer.

Embryo manipulation

Adult wild-caught *Ciona intestinalis* (species type A, 'robusta') animals were obtained from M-REP (San Diego, CA, USA). Protocols for fertilization, dechorionation and electroporation have been described (Christiaen et al., 2009a,b). Plasmid concentration for electroporation varied between 15 and 50 µg per plasmid. For experiments with fixed embryos, healthy embryos were hand-chosen during gastrulation then fixed at the appropriate stage for analysis of neurulation phenotypes. For drug treatments, both UO126 (Promega) and aphidicolin (Promega) were resuspended in DMSO and diluted to 10 µM in filtered artificial seawater (FASW). Embryos were fixed in MEM-FA (3.7% formaldehyde, 0.1 M MOPS pH7.4, 0.5 M NaCl, 1 mM EGTA, 2 mM $MgSO_4$, 0.05% Triton X-100) for 20 min at room temperature, and then washed several times in PBTT (PBS containing 50 mM NH_4Cl and 0.3% Triton X-100) and PBTr (PBS containing 0.01% Triton X-100). For phalloidin staining, embryos were incubated overnight at 4°C with Alexa Fluor 488-conjugated phalloidin (Molecular Probes; 1:500) in PBTr, and then rinsed with PBS containing 0.005% Triton X-100. Embryos were then equilibrated in 50% glycerol in PBS with 2% DABCO and left to settle in a glass coverslip bottom dish allowing them to be manually oriented prior to imaging. Only embryos exhibiting non-mosaic expression of reporter genes in A-line neural cells were included in analyses. Imaging was performed on inverted Zeiss 700 and 780 laser scanning confocal microscopes.

Time-lapse live imaging and cell tracing

For live, time-lapse experiments, embryos were reared in FASW and imaged on glass coverslip bottom dishes at 60 s intervals. Only experiments with good overall embryo health were included in our analysis although some issues were tolerated, particularly minor DNA bridging between cells, which frequently occurred during cell division and seemed to be a largely unavoidable consequence of the electroporation/histone reporter/laser scanning confocal live-imaging experimental scheme. Table S1 shows the outcome of time-lapse experiments performed for this project. Occasionally, embryos drifted and had to be repositioned. Confocal slices

Development (2016) 143, 4665-4675 doi:10.1242/dev.144733

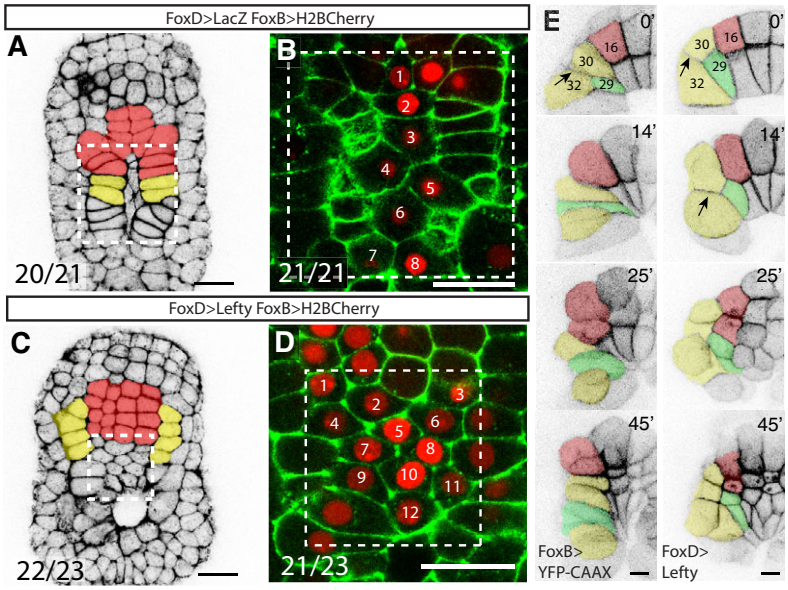

Fig. 9. Stacking defects caused by Nodal inhibition. (A-D) Embryos electroporated with the indicated transgenes and fixed at the mid-neurula stage. (A,C) False-colored, phalloidin-stained embryos with *n* value indicating the number of embryos exhibiting four (A) or six (C) A-line cell columns. (B,D) Counting of floor plate cells. Dashed box indicates the same region of embryo as shown in A,C. Number of embryos with eight (B) or 12 (C) floor plate cells is indicated. Totals are from two independent experiments. Scale bars: 25 µm. (E) False-colored stills from time-lapse live imaging of embryos electroporated with FoxB>YFP-CAAX alone (left) or in combination with FoxD>Lefty (right). Arrows indicate junction between A9.30 and A9.32. Scale bars: 10 µm.

were taken at 1.5-µm intervals through the developing CNS from the dorsal side. The Fiji Trackmate plugin (Schindelin et al., 2012) was used to track cells manually and generate lineage trees and labeled movies. For cases in which tracking was straightforward a maximum projection was generated prior to labeling cells, whereas in other cases cells were labeled on a slice-by-slice basis and a maximum projection was later created for display purposes.

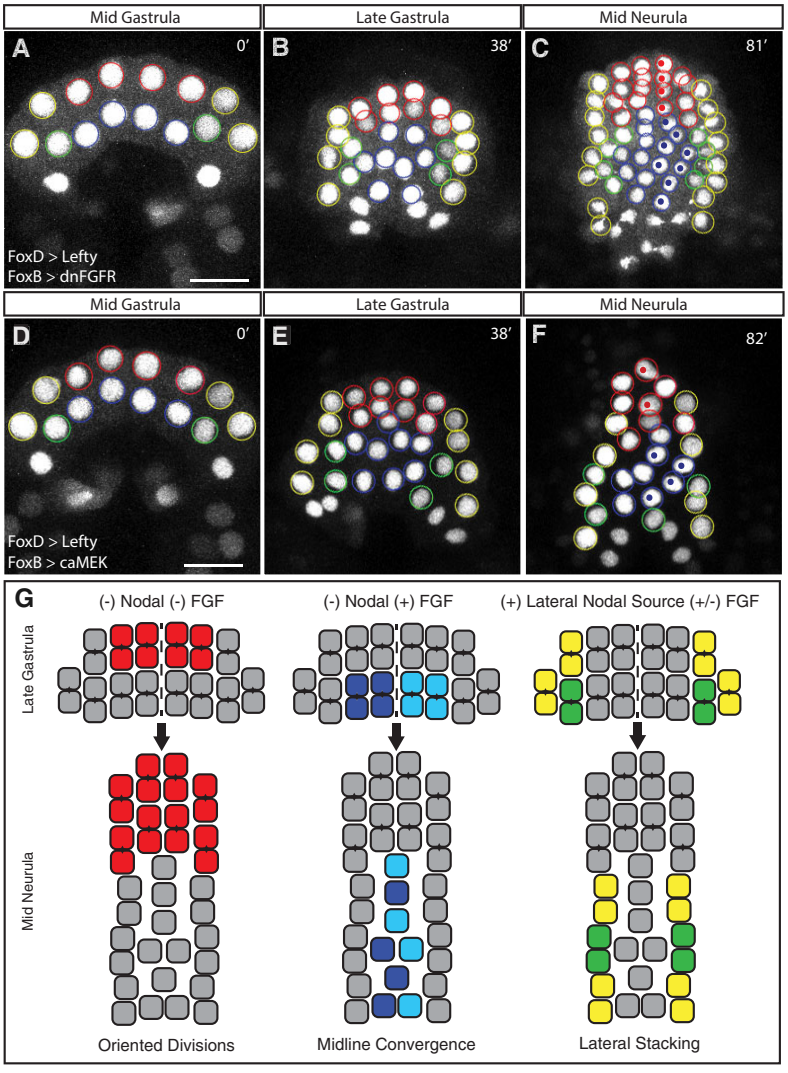

Fig. 10. Oriented divisions are a morphogenetic ground state for the A-line neural lineage, which is modified by FGF/MAPK and Nodal signaling. (A-F) Stills from time-lapse live imaging of embryos electroporated with the indicated transgenes and FoxB>H2B:YFP reporter. Cell lineages are color coded as in Fig. 1B. Where cells from the left and right sides of the embryo mix, right side cells are indicated by a dot within the nucleus. (B,E) Late gastrula stage embryos exhibit similar phenotypes in the presence and absence of FGF/MAPK signaling. (C) Combined Nodal and FGF inhibition causes all A-line neural cells to enter the tenth generation within the same 15 min window (*n*=5/6) and enter 11th generation by mid-neurula stage without midline convergence or lateral stacking (*n*=6/6). (F) When MAPK signaling is activated in the absence of Nodal signaling all cells enter the tenth generation within the same 15 min window (*n*=3/6) and no cells enter the 11th generation by the mid-gastrula stage (*n*=4/7). Ectopic intercalations are present among both medial and lateral cells (*n*=4/7). (G) Visual summary of findings. Top row: At the late gastrula stage, cells have entered the tenth generation via an anterior-posterior oriented division and are positioned next to their sister cells. Midline is indicated by a dashed line. Bottom row: In the absence of earlier Nodal and FGF signals, cells divide again in an anterior-posterior orientation maintaining their position relative to the midline. When MAPK is activated in the absence of Nodal, cells delay their division and converge at the midline becoming separate from their sister cells. If cells have received a Nodal signal, entry into the 11th generation is delayed and cells form lateral stacks without losing contact with their tenth generation sisters. Opposing arrowheads between cells indicate the most recent cell division.

Development (2016) 143, 4665-4675 doi:10.1242/dev.144733

Quantification of 11th generation cells

To quantify the number of 11th generation A9.14 and A9.13 derivatives, FoxB>H2B:Cherry-electroporated embryos were fixed at the mid-neurula stage and stained with phalloidin. By carefully counting the total number of A-line neural cells present and examining their relative positions we were able to determine how many A9.14/13-derived cells were present in each embryo, and thus infer the number of 11th generation cells.

Membrane length analysis

Confocal microscopy was used to image a total of 90 non-mosaic embryos (46 controls and 44 expressing FoxB>caMEK) from four independent experiments. In each experiment, healthy *lacZ*- and caMEK-electroporated embryos were collected prior to the late gastrula stage, at which point some embryos from each group were treated with aphidicolin to prevent A-line cells from reaching the 11th generation. Embryos were then fixed at the mid-neurula stage. Before imaging, embryos were manually oriented such that their dorsal side faced the objective and a confocal stack through neurulating cells was acquired at <1-µm intervals. For embryos treated with aphidicolin a slice best representing the midway point between apical and basal surfaces of A9.14-derived cells was then chosen for each embryo. We then used ImageJ to trace the phalloidin membrane staining on this slice starting from the midline where a-line derivatives intersect A9.14-derived cells anteriorly and ending at the midline where A9.14 cells intersect A9.13 derivatives. The ImageJ 'measure' command was used to calculate the length of the traced membrane. For cases in which the shortest span was ambiguous both were measured and the shorter possible span was used. A *P*-value comparing *lacZ* +aphidicolin and caMEK+aphidicolin membrane lengths was calculated using the Wilcoxon two-sample test and box plots were generated using BoxPlotR web tool. Embryos in which cell identity was ambiguous or an A9.14-derived cell had entered the 11th generation despite aphidicolin treatment were excluded from the membrane length analysis.

Acknowledgements

We thank Shigeki Fujiwara for FoxD>Lefty and FoxD>Nodal constructs and members of the Levine and Harland labs for helpful discussions. I.A.N. also thanks Richard Harland for providing invaluable guidance during the completion of this study.

Competing interests

The authors declare no competing or financial interests.

Author contributions

I.A.N. designed and performed the experiments and wrote the manuscript in consultation with M.L.

Funding

This work was funded by a grant from the National Institutes of Health [NS 076542 to M.L.] and a National Institutes of Health NRSA Trainee appointment (T32). Deposited in PMC for release after 12 months.

Supplementary information

Supplementary information available online at
http://dev.biologists.org/lookup/doi/10.1242/dev.144733.supplemental

References

Bertrand, V., Hudson, C., Caillol, D., Popovici, C. and Lemaire, P. (2003). Neural tissue in ascidian embryos is induced by FGF9/16/20, acting via a combination of maternal GATA and Ets transcription factors. *Cell* **115**, 615-627.

Böttcher, R. T. and Niehrs, C. (2005). Fibroblast growth factor signaling during early vertebrate development. *Endocr. Rev.* **26**, 63-77.

Christiaen, L., Wagner, E., Shi, W. and Levine, M. (2009a). Isolation of sea squirt (Ciona) gametes, fertilization, dechorionation, and development. *Cold Spring Harb. Protoc.* **2009**, pdb.prot5344.

Christiaen, L., Wagner, E., Shi, W. and Levine, M. (2009b). Electroporation of transgenic DNAs in the Sea Squirt Ciona. *Cold Spring Harb. Protoc.* **2009**, pdb. prot5345.

Cole, A. G. and Meinertzhagen, I. A. (2004). The central nervous system of the ascidian larva: mitotic history of cells forming the neural tube in late embryonic Ciona intestinalis. *Dev. Biol.* **271**, 239-262.

Conklin, E. G. (1905). The organization and cell-lineage of the ascidian egg. *Proc. Acad. Nat. Sci. Philadelphia* **13**, 1-119.

Corbo, J. C., Erives, A., Di Gregorio, A., Chang, A. and Levine, M. (1997). Dorsoventral patterning of the vertebrate neural tube is conserved in a protochordate. *Development* **124**, 2335-2344.

Davidson, B., Shi, W., Beh, J., Christiaen, L. and Levine, M. (2006). FGF signaling delineates the cardiac progenitor field in the simple chordate, Ciona intestinalis. *Genes Dev.* **4**, 2728-2738.

Delsuc, F., Brinkmann, H., Chourrout, D. and Philippe, H. (2006). Tunicates and not cephalochordates are the closest living relatives of vertebrates. *Nature* **439**, 965-968.

Di Gregorio, A., Harland, R. M., Levine, M. and Casey, E. S. (2002). Tail morphogenesis in the ascidian, Ciona intestinalis, requires cooperation between notochord and muscle. *Dev. Biol.* **244**, 385-395.

Ettensohn, C. A. (2013). Encoding anatomy: developmental gene regulatory networks and morphogenesis. *Genesis* **51**, 383-409.

Gainous, T. B., Wagner, E. and Levine, M. (2015). Diverse ETS transcription factors mediate FGF signaling in the Ciona anterior neural plate. *Dev. Biol.* **399**, 218-225.

Hashimoto, H., Enomoto, T., Kumano, G. and Nishida, H. (2011). The transcription factor FoxB mediates temporal loss of cellular competence for notochord induction in ascidian embryos. *Development* **138**, 2591-2600.

Hashimoto, H., Robin, F. B., Sherrard, K. M. and Munro, E. M. (2015). Sequential contraction and exchange of apical junctions drives zippering and neural tube closure in a simple chordate. *Dev. Cell* **32**, 241-255.

Hudson, C. and Yasuo, H. (2005). Patterning across the ascidian neural plate by lateral Nodal signalling sources. *Development* **132**, 1199-1210.

Hudson, C., Lotito, S. and Yasuo, H. (2007). Sequential and combinatorial inputs from Nodal, Delta2/Notch and FGF/MEK/ERK signalling pathways establish a grid-like organisation of distinct cell identities in the ascidian neural plate. *Development* **134**, 3527-3537.

Hudson, C., Sirour, C. and Yasuo, H. (2015). Snail mediates medial-lateral patterning of the ascidian neural plate. *Dev. Biol.* **403**, 172-179.

Imai, K. S., Hino, K., Yagi, K., Satoh, N. and Satou, Y. (2004). Gene expression profiles of transcription factors and signaling molecules in the ascidian embryo: towards a comprehensive understanding of gene networks. *Development* **131**, 4047-4058.

Imai, K. S., Levine, M., Satoh, N. and Satou, Y. (2006). Regulatory blueprint for a chordate embryo. *Science* **312**, 1183-1187.

Imai, K. S., Stolfi, A., Levine, M. and Satou, Y. (2009). Gene regulatory networks underlying the compartmentalization of the Ciona central nervous system. *Development* **136**, 285-293.

Kim, G. J. and Nishida, H. (2001). Role of the FGF and MEK signaling pathway in the ascidian embryo. *Dev. Growth Differ.* **43**, 521-533.

Lemaire, P., Bertrand, V. and Hudson, C. (2002). Early steps in the formation of neural tissue in ascidian embryos. *Dev. Biol.* **252**, 151-169.

Lumsden, A. and Krumlauf, R. (1996). Patterning the vertebrate neuraxis. *Science* **274**, 1109-1115.

Mansour, S. J., Matten, W. T., Hermann, A. S., Candia, J. M., Rong, S., Fukasawa, K., Vande Woude, G. F. and Ahn, N. G. (1994). Transformation of mammalian cells by constitutively active MAP kinase kinase. *Science* **265**, 966-970.

Mita, K. and Fujiwara, S. (2007). Nodal regulates neural tube formation in the Ciona intestinalis embryo. *Dev. Genes Evol.* **217**, 593-601.

Mita, K., Koyanagi, R., Azumi, K., Sabau, S. V. and Fujiwara, S. (2010). Identification of genes downstream of nodal in the Ciona intestinalis embryo. *Zool. Sci.* **27**, 69-75.

Miyamoto, D. M. and Crowther, R. J. (1985). Formation of the notochord in living ascidian embryos. *J. Embryol. Exp. Morphol.* **86**, 1-17.

Nakamura, M. J., Terai, J., Okubo, R., Hotta, K. and Oka, K. (2012). Three-dimensional anatomy of the Ciona intestinalis tailbud embryo at single-cell resolution. *Dev. Biol.* **372**, 274-284.

Nakatani, Y. and Nishida, H. (1997). Ras is an essential component for notochord formation during ascidian embryogenesis. *Mech. Dev.* **68**, 81-89.

Nicol, D. and Meinertzhagen, I. A. (1988a). Development of the central nervous system of the larva of the Ascidian, Ciona intestinalis L. II. Neural plate morphogenesis and cell lineages during neurulation. *Dev. Biol.* **130**, 737-766.

Nicol, D. and Meinertzhagen, I. A. (1988b). Development of the central nervous system of the larva of the ascidian, Ciona intestinalis L. I. The early lineages of the neural plate. *Dev. Biol.* **130**, 721-736.

Nicol, D. and Meinertzhagen, I. A. (1991). Cell counts and maps in the larval central nervous system of the ascidian Ciona intestinalis (L.). *J. Comp. Neurol.* **309**, 415-429.

Nishida, H. (1987). Cell lineage analysis in ascidian embryos by intracellular injection of a tracer enzyme. III. Up to the tissue restricted stage. *Dev. Biol.* **121**, 526-541.

Nishimura, T., Honda, H. and Takeichi, M. (2012). Planar cell polarity links axes of spatial dynamics in neural-tube closure. *Cell* **149**, 1084-1097.

Noda, T. and Satoh, N. (2008). A comprehensive survey of cadherin superfamily gene expression patterns in Ciona intestinalis. *Gene Expr. Patterns* **8**, 349-356.

Ogura, Y., Sakaue-Sawano, A., Nakagawa, M., Satoh, N., Miyawaki, A. and Sasakura, Y. (2011). Coordination of mitosis and morphogenesis: role of a prolonged G2 phase during chordate neurulation. *Development* **138**, 577-587.

Schindelin, J., Arganda-Carreras, I., Frise, E., Kaynig, V., Longair, M., Pietzsch, T., Preibisch, S., Rueden, C., Saalfeld, S., Schmid, B. et al. (2012). Fiji: an open-source platform for biological-image analysis. *Nat. Methods* **9**, 676-682.

Development (2016) 143, 4665-4675 doi:10.1242/dev.144733

Shi, W., Peyrot, S. M., Munro, E. and Levine, M. (2009). FGF3 in the floor plate directs notochord convergent extension in the Ciona tadpole. *Development* **136**, 23-28.

Shindo, A. and Wallingford, J. B. (2014). PCP and septins compartmentalize cortical actomyosin to direct collective cell movement. *Science* **343**, 649-652.

Stolfi, A. and Levine, M. (2011). Neuronal subtype specification in the spinal cord of a protovertebrate. *Development* **138**, 995-1004.

Stolfi, A., Ryan, K., Meinertzhagen, I. A. and Christiaen, L. (2015). Migratory neuronal progenitors arise from the neural plate borders in tunicates. *Nature* **527**, 371-374.

Takeuchi, M., Nakabayashi, J., Sakaguchi, T., Yamamoto, T. S., Takahashi, H., Takeda, H. and Ueno, N. (2003). The prickle-related gene in vertebrates is essential for gastrulation cell movements. *Curr. Biol.* **13**, 674-679.

Taniguchi, K. and Nishida, H. (2004). Tracing cell fate in brain formation during embryogenesis of the ascidian Halocynthia roretzi. *Dev. Growth Differ.* **46**, 163-180.

Veeman, M. T., Newman-Smith, E., El-Nachef, D. and Smith, W. C. (2010). The ascidian mouth opening is derived from the anterior neuropore: reassessing the mouth/neural tube relationship in chordate evolution. *Dev. Biol.* **344**, 138-149.

Wagner, E. and Levine, M. (2012). FGF signaling establishes the anterior border of the Ciona neural tube. *Development* **139**, 2351-2359.